JACS
JOURNAL OF THE AMERICAN CHEMICAL SOCIETY
Article
pubs.acs.org/JACS

Magnetic Tuning of All-Organic Binary Alloys between Two Stable Radicals

Gonca Seber,[†] Rafael S. Freitas,*[,‡] Joel T. Mague,[§] Armando Paduan-Filho,[‡] Xavier Gratens,[‡] Valdir Bindilatti,[‡] Nei Fernandes Oliveira, Jr.,[‡] Naoki Yoshioka,[∥] and Paul M. Lahti*[,†]

[†]Department of Chemistry, University of Massachusetts, Amherst, Massachusetts 01003, United States
[‡]Instituto de Física, Universidade de São Paulo, C.P. 66318−05314-970 São Paulo, SP, Brazil
[§]Department of Chemistry, Tulane University, New Orleans, Louisiana 70118, United States
[∥]Department of Applied Chemistry, Keio University, Yokohama 223-8522, Japan

Supporting Information

ABSTRACT: Mixtures of 2-(4,5,6,7-tetrafluorobenzimidazol-2-yl)-4,4,5,5-tetramethyl-4,5-dihydro-1*H*-imidazole-3-oxide-1-oxyl (F4BImNN) and 2-(benzimidazol-2-yl)-4,4,5,5-tetramethyl-4,5-dihydro-1*H*-imidazole-3-oxide-1-oxyl (BImNN) crystallize as solid solutions (alloys) across a wide range of binary compositions. $(F4BImNN)_x(BImNN)_{(1-x)}$ with $x < 0.8$ gives orthorhombic unit cells, while $x \geq 0.9$ gives monoclinic unit cells. In all crystalline samples, the dominant intermolecular packing is controlled by one-dimensional (1D) hydrogen-bonded chains that lead to quasi-1D ferromagnetic behavior. Magnetic analysis over 0.4−300 K indicates ordering with strong 1D ferromagnetic exchange along the chains (J/k = 12−22 K). Interchain exchange is estimated to be 33- to 150-fold weaker, based on antiferromagnetic ordered phase formation below Néel temperatures in the 0.4−1.2 K range for the various compositions. The ordering temperatures of the orthorhombic samples increase linearly as $(1 - x)$ increases from 0.25 to 1.00. The variation is attributed to increased interchain distance corresponding to decreased interchain exchange, when more F4BImNN is added into the orthorhombic lattice. The monoclinic samples are not part of the same trend, due to the different interchain arrangement associated with the phase change.

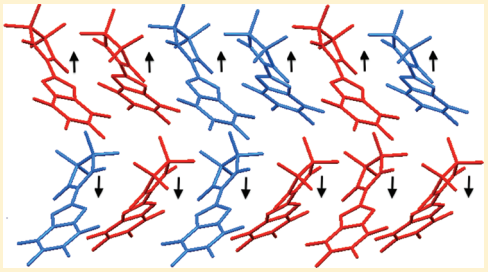

1. INTRODUCTION

Control of magnetic exchange interactions in molecule-based materials by tuning their crystallographic packing is a much-pursued endeavor in soft matter materials, such as organic molecular solids.[1] Some short-range crystal assembly geometries are predictable when strongly directional intermolecular forces are involved, such as hydrogen bonds. However, general predictions of lattice packing in organic molecular crystals based only on structure are still not possible. Even subtle changes in intermolecular packing of radicals based solely on the upper row elements can give major changes in qualitative magnetic behavior, since exchange in these systems is significant only over distances less than 5 Å between sites with large absolute spin density magnitudes. Although strong exchange interactions require intermolecular spin orbital overlap, overall magnetism in organic materials can also depend crucially on small interactions involving close contacts between small spin density sites or on more generalized dipole−dipole interactions. This makes magnetostructural comparisons difficult for materials composed of different molecules, because their crystallographies frequently are quite different.

Comparisons are clearer between crystallographically isomorphous materials. One type of variable composition material with strong potential to have the same or very similar crystallography is the class of solid solutions ("alloys"). These offer opportunities to study full phase diagrams of magnetic and crystallographic behavior as functions of composition, with enough similarity of solid-state packing behavior to allow clearer comparisons between compositionally different materials. A few studies of organic radical alloy-type mixtures have been previously reported. The dilution by Awaga, Sugano, and Kinoshita of galvinoxyl radical with its diamagnetic precursor, hydrogalvinoxyl, was one of the first demonstrations of organic radical solid solutions.[2] Mukai and co-workers similarly studied dilution[3] of an oxoverdazyl TOV with its diamagnetic precursor TOV-H. They also investigated the variation of magnetic behavior in binary alloys, using pairs of radicals: p-CDpOV with p-BDpOV,[4] and p-CyDOV with p-CyDTV (see Chart 1 for structures).[5] The latter two sets of studies are the major body of published work for purely organic radical/radical alloys. They utilized powder X-ray diffraction (XRD) to determine variation in unit cell parameters: changes in specific intermolecular contacts were not available from this.

A preliminary study with full single-crystal XRD determination was previously reported[6] for a 1:1 solid solution between 2-(4,5,6,7-tetrafluorobenzimidazol-2-yl)-4,4,5,5-tetramethyl-4,5-dihydro-1*H*-imidazole-3-oxide-1-oxyl and 2-(benzimidazol-

Received: November 7, 2011
Published: February 9, 2012

Downloaded via UNIV OF SAO PAULO on June 28, 2023 at 15:06:54 (UTC).
See https://pubs.acs.org/sharingguidelines for options on how to legitimately share published articles.

 © 2012 American Chemical Society dx.doi.org/10.1021/ja2104697 | *J. Am. Chem. Soc.* 2012, 134, 3825−3833

Chart 1

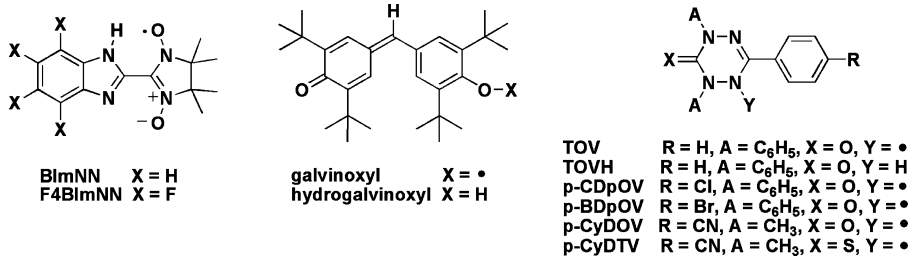

2-yl)-4,4,5,5-tetramethyl-4,5-dihydro-1*H*-imidazole-3-oxide-1-oxyl, F4BImNN and BImNN, respectively. Both the intermolecular crystal packing and the exchange behaviors were similar to those observed[6−9] in the pure individual components. Although F4BImNN and BImNN are not isomorphous, they form geometrically very similar hydrogen-bonded chains; so does the 1:1 solid solution. A point of particular interest for all of these samples is the strong one-dimensional (1D) ferromagnetic (FM) exchange interactions associated with chain formation in each. Because of this, and because the individual components exhibit such similar intermolecular packing, we decided to test the magneto-structural behavior of a wide range of F4BImNN/BImNN binary mixture ratios.

In this article, we report single-crystal XRD analyses and magnetic studies for a full range of binary solid solutions, or alloys, as they will be subsequently called in this article, between F4BImNN and BImNN, $(F4BImNN)_x(BImNN)_{(1-x)}$ with $0 < x < 1$. Single-crystal XRD gives a much more detailed picture than lattice-only powder XRD for variation of intermolecular packing in the $(F4BImNN)_x(BImNN)_{(1-x)}$ alloys with composition, including a crystal lattice phase change. Low temperature magnetism studies for all of the samples show ordering at temperatures that were tunable with regular trends over much of the composition range, to the point that the magnetic ordering temperature of pure BImNN was successfully predicted before it was measured. The results constitute a comprehensive structure−property study relating magnetic ordering temperature to composition in a set of closely related, purely organic, radical/radical magnetic alloys.

2. MATERIALS AND METHODS

2.1. Synthesis. F4BImNN[7] and BImNN[8] were synthesized using literature procedures. Their purities were confirmed by high pressure liquid chromatography (HPLC). Details are given in the Supporting Information.

2.2. Sample Preparation and Characterization. F4BImNN was crystallized from acetonitrile. BImNN and binary mixtures between F4BImNN and BImNN were dissolved in chloroform and allowed to crystallize slowly by diffusion of hexane vapor into the solutions at ambient temperature in sealed containers. Individual crystals of the mixture solids were tested by HPLC, which showed consistently very similar component ratios for a given sample. Samples also were checked by comparing XRD unit cell parameters at room temperature for multiple single crystals selected from each sample; these also showed the tested crystals to be in the same phase for each given sample. For a few sample $(F4BImNN)_x(BImNN)_{(1-x)}$ compositions $x \sim 0.8-0.9$, diffraction grade crystals did not form to a significant extent.

The alloy solids were also analyzed by thermogravimetric analysis (TGA) under nitrogen and by FT-ATR infrared spectroscopy. TGA decomposition temperatures T_d were taken as the first, relatively sharp maximum of the derivative of the data: some compositions also showed more generalized, broad temperature range decomposition processes for $T > 275$ °C.

2.3. Crystallography. Single crystals were analyzed by XRD at 100 K (Tulane); in several cases, crystals from the same sample were also analyzed at room temperature (UMass Amherst). Low temperature lattice parameters are given in the main text, and room temperature lattice parameters are given in the Supporting Information for the pure components and some of the binary alloys. Full crystallographic details for all samples are given in the Supporting Information.

For the low temperature analyses, full spheres of data were collected on a Bruker-AXS Smart APEX CCD diffractometer using a combination of ω and φ scans with scan widths varying between 0.3°and 0.5°, and exposure times chosen to provide the maximum possible numbers of observable diffraction maxima. The raw intensity data were converted to F^2 values with SAINT,[10] and at the same time, a global refinement of unit cell parameters was performed. Empirical absorption corrections and merging of symmetry equivalent reflections were performed with SADABS.[11] The structures were solved by direct methods (SHELXS) and refined by full-matrix least-squares procedures (SHELXL).[12] In most instances, at least some of the hydrogen atoms could be observed. Those attached to carbon were placed in idealized positions while those attached to nitrogen (in the alloys) were placed in positions derived from difference maps; all were included as riding contributions with isotropic displacement parameters tied to those of the attached atoms.

2.4. Magnetic Measurements. Magnetic dc-susceptibility measurements were carried out over 1.8−300 K using a Quantum Design MPMS-7 magnetometer in dc mode. Molar susceptibilities are given in units of $emu \cdot Oe^{-1} \cdot mol^{-1}$; the numerical values are the same as would arise if a commonly used alternative scheme of units, $cm^3 \cdot mol^{-1}$, were used instead. Magnetization versus field data were obtained at a fixed temperature of 1.8 K on the same instrument. Polycrystalline samples were placed into gelatin capsules and held in place with a plug of cotton. Temperature independent corrections were made by extrapolation from the higher temperature raw susceptibilities. Ac-susceptibility measurements at 0.4−1.8 K were carried out on polycrystalline samples in PVC sample holders using a custom-built apparatus that has been described[13] elsewhere. Specific mathematical models used to interpret susceptibility versus temperature and magnetization versus field data are given in the text below, and in detail in the Supporting Information.

3. RESULTS AND DISCUSSION

At most compositions, diffraction quality crystals of the organic radical alloys formed readily. Fluorine-rich samples formed fairly large, blue-black prisms, while fluorine-poor mixtures yielded clusters of fine needles. HPLC of dissolved individual crystals from each sample showed good quantitative agreement with the input component ratios, to within a few percent. Thermogravimetric analysis (TGA) of the mixtures each showed single macroscopic decomposition temperatures T_d, consistent with a single alloy phase rather than mixtures of different phases having different decomposition points.

dx.doi.org/10.1021/ja2104697 | J. Am. Chem. Soc. 2012, 134, 3825−3833

Table 1. Selected Properties of $(F4BImNN)_x(BImNN)_{(1-x)}$ Alloys

fraction of F4BImNN[a]	space group [Z][b]	V/Å^3	a, b, c/Å[c]	β (deg)	$T_N(0)$/K[d]	T_d/°C[e]	J/k (θ)[f]
1.00	$P2_1/c$ [4]	1454.7(3)	8.5019(11) 20.951(3) **8.7237(12)**	110.586(2)	0.761	172	22 K[g]
0.95	$P2_1/c$ [4]	1441.1(4)	8.4721(13) 20.890(3) **8.7019(13)**	110.650(2)	0.64	*	*
0.90	$P2_1/c$ [4]	1424.5(12)	8.436(4) 20.805(11) **8.676(4)**	110.680(8)	0.74, 0.705	175	18 K (0.2 K)
0.88	*Pbca* [8]	2880.5(10)	**8.8193(17)** 15.674(3) 20.839(4)	90.000	0.62	*	*
0.75	*Pbca* [8]	2848.4(4)	**8.7678(7)** 15.6310(12) 20.7838(16)	90.000	0.49, 0.50	187	12 (0.1)
0.50	*Pbca* [8]	2770.2(14)	**8.694(3)** 15.491(4) 20.569(6)	90.000	0.726	196	15 (0.3)
0.25	*Pbca* [8]	2709.2(5)	**8.6527(8)** 15.3511(15) 20.396(2)	90.000	0.94, 0.95	206	13 (0.6)
0.17	*Pbca* [8]	2695.4(4)	**8.6503(8)** 15.3100(14) 20.3524(18)	90.000	0.97	213	*
0.10	*Pbca* [8]	2687.7(19)	**8.651(4)** 15.285(6) 20.327(8)	90.000	1.05, 1.06	217	16 (0.7)
0.00	*Pbca* [8][h]	2651.3(3)	**8.6236(6)** 15.2101(10) 20.2137(13)	90.000	1.16	225	22[i]

[a] $(F4BImNN)_x(BImNN)_{(1-x)}$ solid solution composition *x*. [b] All unit cell parameters obtained at 100 K. [c] Boldface numbers indicate the axis along which Scheme 1 FM exchange chain propagates. [d] Neél temperatures from zero field ac-measured χ vs *T* maxima. Double entries indicate duplicate measurements for independent samples. [e] Decomposition temperatures determined as the maximum of a derivative plot of thermogravimetric mass loss versus temperature. [f] Exchange constants and mean field terms in Kelvin (K) from fitting χ*T* vs *T* data in a dc external field of 1000 Oe with the Padé 1D chain model described in the text. [g] Ref 7, evaluated without mean field. [h] From CCDC CIF entry REFXUV. [i] Ref 8, evaluated without mean field. *Not evaluated.

Single-crystal XRD analyses at 100 K confirmed formation of solid solutions, with F4BImNN or BImNN occupying random sites in a common lattice, in ratios quite close to the input composition ratios. The unit cell lattice parameters at each $(F4BImNN)_x(BImNN)_{(1-x)}$ composition are given in Table 1, as well as those for pure F4BImNN and pure BImNN; more complete summaries at room temperature and 100 K are given in the Supporting Information. The lattice volume contractions found upon cooling from room temperature to 100 K were 3.0−3.5%. The $(F4BImNN)_x(BImNN)_{(1-x)}$ compositions with $x = 0.90-1.00$ crystallized in the monoclinic $P2_1/c$ space group; those with $x = 0.0-0.75$ crystallized in the orthorhombic *Pbca* space group. Samples with $x \sim 0.8-0.9$ tended not to give diffraction quality single crystals but bundles of fibers that diffracted poorly if at all. A sample with $x = 0.83$ yielded some crystals with an orthorhombic space group (see the Supporting Information). However, as will be described below, samples of this composition gave anomalous magnetism, which we attribute to a lack of a consistent crystalline phase formation throughout the sample bulk.

Figure 1 compares corresponding views of alloy monoclinic and orthorhombic lattices viewed looking down the axis along which hydrogen-bonded chains form. It is convenient to compare analogous packing motifs among the samples, specifically the hydrogen-bonded stacking axis (herein, also called the FM stacking axis for reasons described below), a "butterfly" packing axis that roughly follows the direction in which the benzimidazole π-electron clouds point, and an interchain contact axis that roughly follows the direction of the benzimidazole ring edges (C−F and C−H bonds). These descriptions will be used to avoid confusion related to the change of axial designations across the orthorhombic−monoclinic phase transition. From the viewpoint of Figure 1, the orthorhombic−monoclinic phase change involves one "slab" of butterfly packed chains slipping vertically relative to the other. In the orthorhombic phase, the interslab contact region involves nearly edge-on aryl−aryl contacts, and methyl−methyl contacts. In the monoclinic phase, the interslab slippage leads to all all aryl−methyl edge-on contacts between chains. A reason for this is suggested later, below.

Magnetic susceptibility measurements at 1.8−300 K were carried out in a dc external field of 1000 Oe. Similarly to the previous reports for pure F4BImNN,[7] BImNN,[8,9] and their equimolar alloy[6] with $x = 0.5$, all samples showed positive Weiss constants from the abscissa intercepts of $1/\chi$ versus *T* plots, and strong upturns in χ*T* versus *T* plots; both features

dx.doi.org/10.1021/ja2104697 | J. Am. Chem. Soc. 2012, 134, 3825−3833

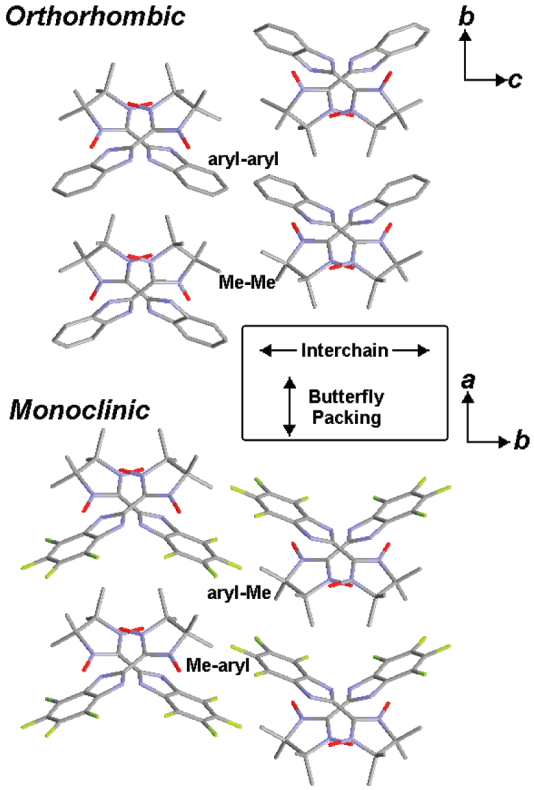

Figure 1. Relationships between packing in orthorhombic and monoclinic alloy phases. Directionality of interchain contacts and butterfly packing are indicated; the ferromagnetic (hydrogen-bonded) stack contacts run into the figure view.

indicate significant FM exchange interactions. Example χT versus T plots are shown in Figure 2; most are for the

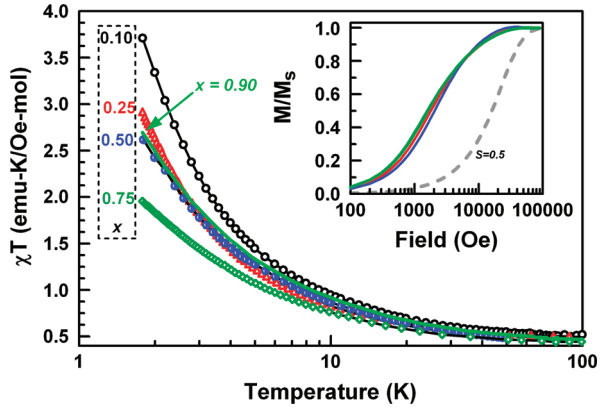

Figure 2. χT vs T plots for selected alloys at 1000 Oe, showing data from 1.8 to 100 K. Inset shows normalized magnetization plots for the same samples (same color coding) at 1.8 K; the theoretical M/M_s vs H Brillouin curve for $S = {}^1/_2$ is shown as a broken line curve.

orthorhombic phases, but $x = 0.9$ data are given to exemplify the similarity of monoclinic to orthorhombic sample magnetic behavior when considering only dc susceptibility above 2 K. From previous studies,[7,8] the FM exchange in F4BImNN and BImNN is attributed to hydrogen-bonded chain assembly of the nitronylnitroxide units into stacks with a favorable spin orbital overlap between large positive spin density on the O atoms and small negative spin density on the radical C atoms. The FM exchange thus comes from the Oα···Cβ spin orbital contacts shown in Scheme 1. Assuming that these contacts

Scheme 1. Spin Orbital Overlap at the Cβ···Oα Contact That Leads to Ferromagnetic Chain Exchange Coupling

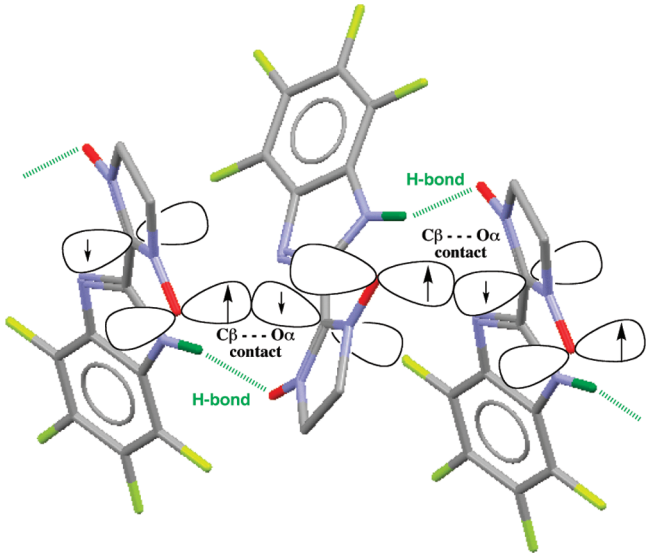

control the polarization of other spin density sites, all N−O units in the chains will have positive α-spin density, producing net FM exchange throughout the chain. Experimentally, F4BImNN, BImNN, and $(F4BImNN)_{0.5}(BImNN)_{0.5}$ have been shown to exhibit exchange constants of J/k = +22 K,[7] +22 K,[8] and +15 K,[6] respectively, all evaluated using the same Padé-type magnetic 1D Heisenberg chain model[14] with $H = -2J\sum S_1 \cdot S_{1+N}$. All of the samples in the present study form the same hydrogen-bonded chains, propagating along the c-axis in the monoclinic samples and the a-axis in the orthorhombic samples. Fitting the χT versus T data for the alloys by the same 1D chain model using fixed $g = 2.006$ also yields relatively large, positive values of J/k, as shown in Table 1 for samples analyzed over 1.8−300 K.

All of the alloy samples in this study also showed magnetization versus field (M vs H) behavior at 1.8 K that fits to spin quantum numbers ranging over $S = 6$−11, based on Brillouin function fitting. Several example M versus H curves at 1.8 K normalized against saturation magnetizations M_s are shown in Figure 2. With limited variation, all of the alloy samples show similar magnetic behavior. This is consistent with assigning an important magnetic role to the highly reproducible hydrogen-bonded chain motif in all of the crystalline alloys, even across the phase change boundary with changing composition. The values of S are much larger than the value of $S = {}^1/_2$ expected for radical spin units, because the spins in the chain are strongly oriented by the intrachain FM exchange coupling. The results reinforce the susceptibility results for the general model whereby the full composition range of crystalline binary alloys over $x = 0.0$−1.0 is magnetically dominated by the strong FM chain intermolecular motif of Scheme 1. The phase change in the fluorine-rich composition region does not much change the dominating intrachain FM 1D chain motif; but, the *interchain* geometry changes, as is discussed below.

Because of the strong intrachain exchange, the alloys can be considered as quasi-1D ferromagnetic materials. Completely isolated 1D exchange coupled chains cannot undergo magnetic

dx.doi.org/10.1021/ja2104697 | J. Am. Chem. Soc. 2012, 134, 3825−3833

ordering throughout the bulk of the sample. However, in practice, many such systems have small interchain exchange interactions that lead to bulk ordering. Murata et al.[7b] previously reported zero-field ac-susceptibility and heat capacity studies showing that pure F4BImNN undergoes bulk ordering as an antiferromagnet with a Néel temperature of $T_N(0)$ = 0.72 K in zero external field. Prior to the present study, this was the only direct *magnetic* observation of the ordering temperature in benzimidazole-functionalized nitronylnitroxides, although Sugano et al. recently reported[15] BImNN to order at 1.0(1) K based on detection of μSR magnetic fluctuations below that temperature.

Several binary F4BImNN/BImNN alloys, as well as pure BImNN, were studied under zero field ac-susceptibility conditions below 2 K at 155 Hz frequency and 10 Oe modulation fields. Pure F4BImNN was previously studied[7b] under similar conditions. All samples showed χ versus T maxima at varying temperatures, except for x = 0.83 mixtures that barely showed a weak feature. The maxima for the other samples behave in a manner consistent with antiferromagnetic Néel transitions, since they shift to lower temperatures in applied external magnetic fields (see Supporting Information). The ordering temperatures at zero field, $T_N(0)$, are listed in Table 1 for all samples subjected to sub 2 K magnetic analysis. Figure 3 shows that the ac susceptibility plots, and Figure 4

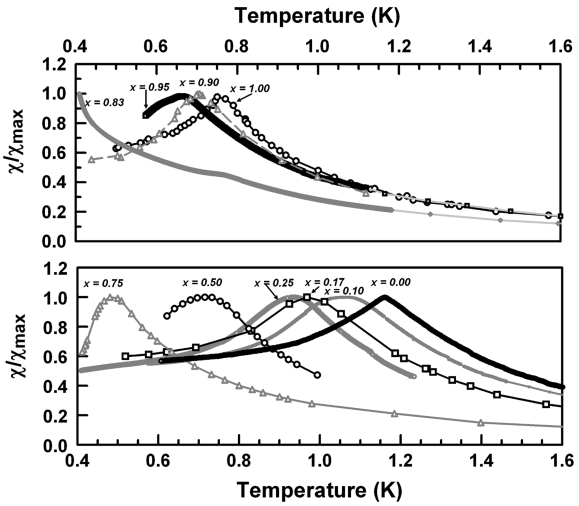

Figure 3. Ac susceptibility χT vs T data for alloys, normalized for each curve to the susceptibility maximum for visual ease of comparison. Upper chart shows fluorine-rich phase region data, lower chart shows only orthorhombic phase data. Data acquired at modulation frequency 155 Hz, modulation amplitude 10 Oe.

shows a plot of zero field $T_N(0)$ as a function of sample composition.

Pure F4BImNN gave $T_N(0)$ = 0.76 K, in good agreement with the previous[7b] report. The variation of the rest of the Néel temperatures with composition is roughly "check mark"-shaped in Figure 4, with a minimum ordering temperature of 0.49 K at x = 0.75. The minimum corresponds to the composition at which the 1D exchange constant J/k in Table 1 is also a minimum, based on the magnetic data above 2 K.

For the monoclinic compositions, $T_N(0)$ roughly decreases in the narrow composition range where this phase is formed as BImNN is added to pure F4BImNN. As described earlier, the behavior of the x = 0.83 phase was anomalous, as seen in

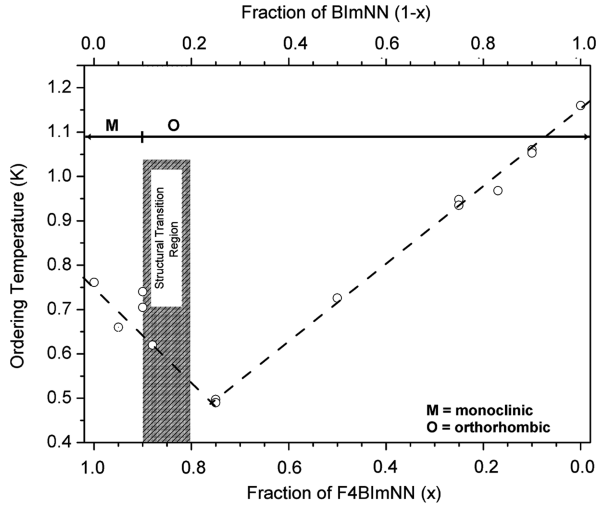

Figure 4. $T_N(0)$ as a function of binary alloy compositions. Gray-hatched zone indicates region of phase change between monoclinic (M) and orthorhombic (O) phases.

multiple samples. The mixture compositions for x = 0.75−0.88 tended to be crystallographically problematic, frequently precipitating into fibrous clusters that did not show good X-ray diffraction. The lack of a clear ordering χ versus T ordering cusp in this composition range is thus attributed to a lack of orderly crystal lattice formation in the bulk of mixtures.

For the orthorhombic compositions, as the fraction of BImNN increases for $(1 - x) > 0.25$, a linear increase in $T_N(0)$ from 0.49 to 1.2 K is observed. The trend is so regular that we could estimate $T_N(0)$ of pure BImNN (nearly the last sample analyzed) based on trends from the rest of the data in Figure 4. The extrapolated estimate turned out to be in good agreement with the μSR-determined ordering temperature[15] from Sugano et al., and with the magnetic results eventually found in this study.

Since interchain exchange is required to get nonzero ordering temperatures, various correlations were considered for sample composition and $T_N(0)$ with various interchain and intermolecular contacts. Figure 5 shows several correlations, using the packing motif nomenclature from Figure 1, plus some additional parameters described below. Monoclinic cell volumes were doubled for appropriate comparison to the corresponding orthorhombic parameters. Of course, the phase change from an orthorhombic to monoclinic space group obscures comparing the nominally corresponding axis lengths across the phase change boundary, especially since the unit cell angle β changes from 90° to 110−111°. But, across the range of compositions, unit cell volume increases almost constantly as fluorine content increases (Figure 5a,b), with a small discontinuity at $(F4BImNN)_x(BImNN)_{(1-x)}$ x = 0.9 corresponding to the phase change boundary. The interchain contact repeat distance increases slowly and monotonically as the fluorine content increases, even across the phase change boundary. The butterfly packing repeat distance sharply lengthens at the phase change boundary as x increases above 0.88, accompanied by a 2.5% decrease in the FM stacking repeat distance length.

Because of the general increase in lattice volumes with increasing fluorine content, the phase change seems reasonably attributable to internal, chemical pressure in the orthorhombic lattice as the content of F4BImNN is increased. As F4BImNN

dx.doi.org/10.1021/ja2104697 | J. Am. Chem. Soc. 2012, 134, 3825−3833

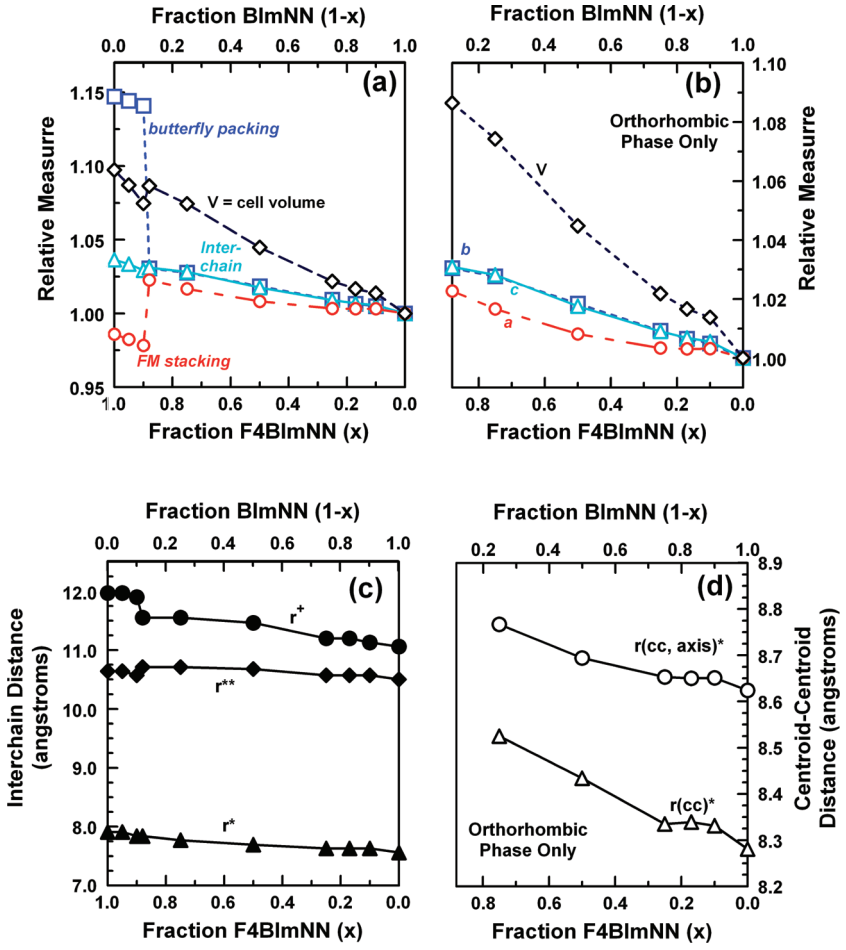

Figure 5. Plots of 100 K lattice parameter relative changes for binary alloys as functions of composition (full range in chart a, orthorhombic phase region in chart b); actual axis to axis (chain to chain) distances from Scheme 3 (chart c); intercentroid distance (Scheme 2 definitions) of *r** interchain pair in Scheme 3, and "down axis" intercentroid distance along a single FM chain, both for orthorhombic phases (chart d).

molecules increasingly replace BImNN and aryl C−F bonds replace C−H bonds in the orthorhombic packing array of Figure 1, the edge-on interchain aryl−aryl contacts should produce increasing repulsion between the partial negative charges on the increasing number of electronegative fluorine atoms. Figure 6 shows a plot of density versus composition from the 100 K crystal analyses, with a linear increase as the F4BImNN content increases in the orthorhombic region. Of course, adding heavier F4BImNN to a nearly constant lattice should increase crystal density; but, F4BImNN also occupies somewhat more volume than BImNN. As a result, increasing crystal density due to increased F4BImNN content should correlate roughly with increased internal chemical pressure. When the F4BImNN content and density get high enough, the phase change from the orthorhombic unit cell occurs with the chains slipping relative to one another along the FM stack axis, to eliminate aryl−aryl edge-on interactions. In the monoclinic phase, the aryl C−F bonds at the periphery of the chains form hydrogen-bond-like aryl−methyl interactions (Figure 1, monoclinic diagram) with the CH_3 groups of the nitronylnitroxides. There are still some moderately close contacts between aryl rings in the monoclinic phase, but they are strongly slip-stacked contacts, not edge-on. Once the monoclinic phase forms and aryl−aryl edge-on steric interactions are eliminated, crystallographic density stabilizes, as shown in Figure 6.

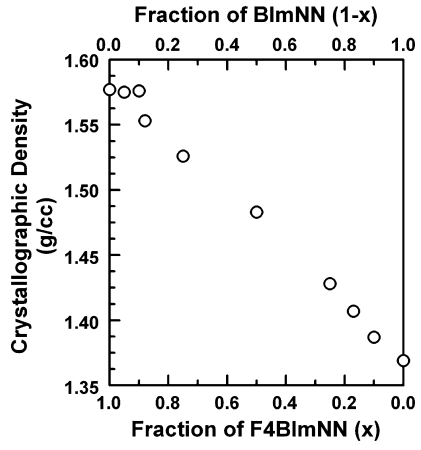

Figure 6. Plot of density versus composition for 100 K crystallographic analyses.

To try to understand the gradual changes of packing with alloy composition, some parameters were desirable to gauge the shifting of chains away from one another, and their slippage relative to one another along the FM stacking direction. Scheme 2 shows a geometric model to describe the interchain distance and translation of one chain versus another along the FM chain propagation direction. The centroids of two

dx.doi.org/10.1021/ja2104697 | J. Am. Chem. Soc. 2012, 134, 3825−3833

Scheme 2. Geometric Parameters within and between Two Hydrogen-Bonded Chains, Compared for Orthorhombic and Monoclinic Alloy Phases

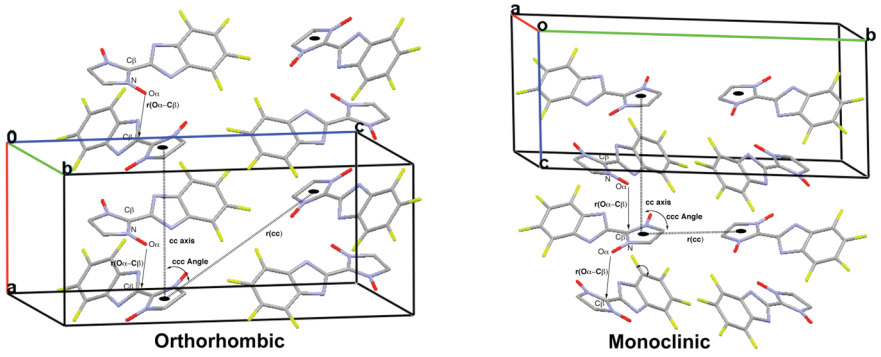

symmetry equivalent nitronylnitroxide rings are convenient reference points to define any FM chain (shown as a "*cc axis*"). A third centroid in a neighboring chain allows description of an interchain distance $r(cc)$, and an angle describing translational "slippage" between different chains ("*ccc angle*").

Of course, the parameters of Scheme 2 depend on which chains are compared. Scheme 3 shows a view similar to Figure

Scheme 3. Interchain Geometry Distances for Orthorhombic Alloy Phases, Looking Down the FM Exchange Interaction Chain Axis[a]

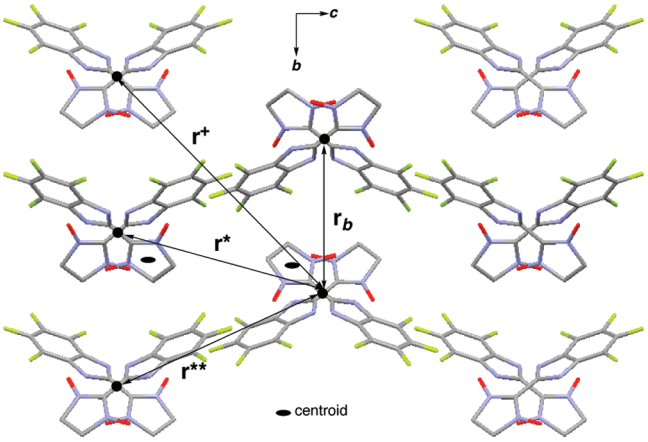

[a]The vector for r_{cc} from Scheme 2 is perpendicular to the figure view; the centroid mark given for one nitronylnitroxide unit shows an example site.

1, straight down the "*cc*" axes of Scheme 2. It shows the spatial relationship between FM chains. Distance r_b correlates directly with the orthorhombic *b* repeat unit distance, while r^*, r^{**}, and r^+ are symmetry-unique chain-to-chain distances relative to any one reference chain, with r^* being the shortest interchain distance. Figure 5c (compare Figure 5b for r_b) shows how these interchain distances increase as the fraction *x* of F4BImNN increases. Figure 5d tracks the *inter*chain geometry slippage between the chains associated by r^* of Scheme 3, with the centroid-centroid distance definition r_{cc} in Scheme 2. Variation of the *intra*chain intermolecular distance $r_{(cc\ axis)}$ is also shown. The interchain distance r_{cc}^* increases by about 0.2 Å, as the *ccc* interchain slippage angle decreases by only about 0.4°. As shown in the various charts of the figure, r_b and $r_{(cc\ axis)}$ also increase within the orthorhombic phases. Across the phase change boundary, r_b and $r_{(cc\ axis)}$ follow the Figure 5a trends of the FM chain and butterfly packing axes as functions of composition.

In the orthorhombic phases, especially, increased distances between chains in the alloys with larger fluorine content correlate well with observed decreases in $T_N(0)$, as shown in Figure 7. But, attributing the $T_N(0)$ variation to *specific*

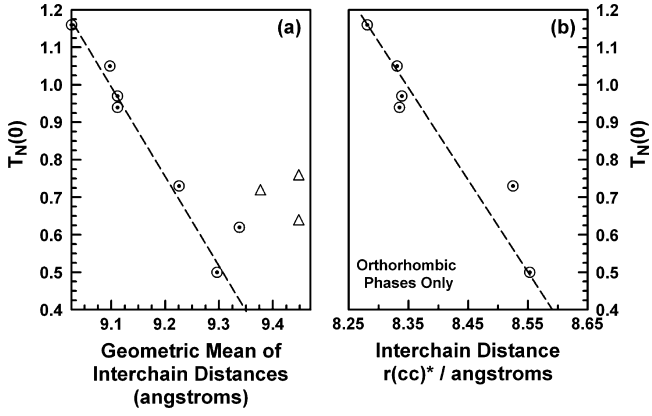

Figure 7. Plots of the Néel temperatures for alloys as functions of the geometric mean of the four interchain distances shown in Scheme 3 (a), and of interchain distance r_{cc}^* (b) for the orthorhombic phases only. For chart (a), circles are for the orthorhombic phases, triangles for monoclinic.

intermolecular contacts is not straightforward. Although the strong FM 1D chain interaction can be assigned with considerable confidence to the specific intermolecular contacts shown in Scheme 1, no close contact exchange pathways *between* chains involve sites of significant or even modest spin density. Almost all of the nitronylnitroxide spin density is confined to the O−N−C−N−O π system, whose smallest density site is (−)16.8% on Cβ of Scheme 1 when computed using the EPR-III method in Gaussian 09;[16] only quite small spin density is computed on the radical unit's methyl groups (<1% each). At the same level of computation, spin density magnitudes are only 0.6−4.3% on the imidazole ring; the benzimidazole benzene ring carbons all have spin density magnitudes of ≤1%. Since both orthorhombic and monoclinic phases order magnetically despite the change in specific intermolecular contacts from the phase change, *no specific intermolecule contacts between chains seem definitively linked to the interchain exchange in any of the alloys.*

A possible explanation for the trends in Figure 4 is that ordering is due to more generalized dipolar interactions

dx.doi.org/10.1021/ja2104697 | J. Am. Chem. Soc. 2012, 134, 3825−3833

between the FM coupled chains of the alloys. One can crudely consider the FM coupled chains as long aspect-ratio magnets that are bundled along their long axes. Minor changes in the interchain distance will affect dipolar exchange between them, and the overall T_N. Figure 6b shows the correlation between $T_N(0)$ and both r_{cc}* and the geometric mean of all of r_b, r*, r**, and r from Scheme 3. The correlations are quite good within the orthorhombic phases but do not hold across the orthorhombic to monoclinic phase transition.

It is possible to gauge roughly the effect of increasing the fraction of F4BImNN on interchain exchange. By using the 1.8−300 K dc susceptibility χT versus T data for several samples across the full range of compositions, and fitting to the 1D ferromagnetic chain model described earlier, the intrachain exchange constants J_{chain}/k = 12−22 K. Equation 1 relates the ordering temperature to intrachain J_{chain} and interchain zJ_{inter} exchange:

$$T_N \approx 2S^2 \cdot (|zJ_{inter}| \cdot J_{chain})^{1/2} \quad (1)$$

If we simplistically assume that the "isolated chain" equivalent 1D FM chain exchange does not vary greatly with composition in the orthorhombic lattices, the apparent variation in the intrachain J/k would arise from variations of interchain exchange. By using eq 1 and fixing the smallest value J_{chain}/k = 12 K, the increase in T_N from 0.49 to 1.05 K as the BImNN content increases from $(1 - x)$ = 0.25 to $(1 - x)$ = 10.00 can be used to estimate that zJ_{inter} increases from ∼0.08 K to ∼0.37 K, about 4.6-fold. By using the assumed J_{chain} = 12 K, J_{chain}/zJ_{inter} ∼ 33−150. This is a very simplified approach, but since zJ_{inter} represents an average over multiple distinct interchain interactions, it is self consistent that the observed small changes to the interchain distances should give such changes in J_{chain}/zJ_{inter} and hence in the ordering temperature.

4. CONCLUSIONS

The binary $(F4BImNN)_x(BImNN)_{(1-x)}$ alloys are truly "crystal engineered" soft materials that allow one to obtain multiple different, but crystallographically analogous samples to tune magnetic behavior as a function of composition in a mixed organic material. The retention of the hydrogen-bonded chain motif found in both pure F4BImNN and BImNN shows the importance of the nitronylnitroxide radical unit as a hydrogen-bond acceptor in these and in the alloys, since Taylor and Lahti showed[17] that 4,5,6,7-tetrafluorobenzimidazole itself has very different crystal packing from benzimidazole[18] itself. Well-defined cocrystal pairings of F4BImNN with BImNN molecules could readily have been imagined as alternatives to the alloys, as is seen in general in many cocrystals of fluoroarenes with hydrocarbon arenes.[19] In a recent case comparable but different in outcome to the work in this article, Rawson and co-workers[20] cosublimed the radicals phenyl-dithiadiazolyl and pentafluorophenyldithiadiazolyl to give specific, 1:1 pairing of the components in a cocrystal.

The $(F4BImNN)_x(BImNN)_{(1-x)}$ set of organic alloys have some of the strongest[15,21] chain-type FM exchange interactions for organic paramagnets based on elements of the upper two rows of the periodic table, as well as being among the most magnetically anisotropic purely organic magnetic materials. Overall, this study provides one of the most detailed magnetostructural analyses of a set of organic all-radical alloys, since full crystal structures, not just unit cell parameters, were obtained at each composition. Although ordering temperatures in the study are relatively low, they are tunable in a regular manner in the orthorhombic portion of the alloy composition phase diagram. If one accepts that variation in the orthorhombic phase alloy packing arises from *internal* crystal pressure effects due to intermolecular repulsions between fluorinated regions of the molecules, and that the packing variation induces the observed changes in ordering temperature, the results of this study can be compared to recently reported[22] effects of *external* pressure on magnetic exchange in pure F4BImNN. The level of control achievable in these all-paramagnetic organic alloy materials encourages further efforts to design and understand analogous materials with similar crystallographic and electronic tunability.

■ ASSOCIATED CONTENT

Supporting Information

General experimental procedures, details of crystallographic analyses, room temperature and 100 K crystallographic data, phase diagram plot of reduced Neél temperatures for several alloys at varying external applied fields, TGA and FTIR for the alloys, spin density computation summary for F4BImNN using the 100 K crystallographic geometry, mathematical equations for magnetic analyses, CIF file summaries of crystallographic data, full citation for ref 16, and Mercury[23] format files allowing manipulation of structures in Figure 1 and Scheme 3. This material is available free of charge via the Internet at http://pubs.acs.org.

■ AUTHOR INFORMATION

Corresponding Author

lahti@chem.umass.edu

Notes

The authors declare no competing financial interest.

■ ACKNOWLEDGMENTS

This material is based upon work supported by the National Science Foundation under grant CHE 0809791 (G.S., P.M.L.; synthesis and characterization of materials). J.T.M. thanks the Chemistry Department of Tulane University for support of the Tulane X-ray Crystallographic Laboratory (crystallography). A.P.F., R.S.F., X.G., V.B., and N.F.O. thank the Fundação de Amparo à Pesquisa do Estado de São Paulo, Brazil (FAPESP - 07/50968-0) for support (sub 2 K magnetometry). G.S. thanks FAPESP for support of her collaborative work at Universidade de São Paulo. We thank a reviewer for suggesting addition of a density versus composition plot.

■ REFERENCES

(1) (a) Miller, J. S.; Gatteschi, D. *Chem. Soc. Rev.* **2011**, *40*, 3053−3368. (b) Rovira, C.; Veciana, J. *CrystEngComm* **2009**, *11*, 2017−2212. (c) *Carbon Based Magnetism: An Overview of the Magnetism of Metal Free Carbon-based Compounds and Materials*; Palacio, F., Makarova, T., Eds.; Elsevier: Amsterdam, Netherlands, 2006. (d) *Magnetism: Molecules to Materials*; Miller, J. S., Drillon, M., Eds.; Wiley-VCH: Weinheim, Germany, 2001−2005; Vols. *1*−*5*. (e) *Molecular Magnetism: New Magnetic Materials*; Itoh, K., Kinoshita, M., Eds.; Gordon & Breach and Kodansha Ltd: Tokyo, Japan, 2000. (f) *Magnetic Properties of Organic Materials*; Lahti, P. M., Ed.; Marcel-Dekker: New York, 1999.

(2) (a) Awaga, K.; Sugano, T.; Kinoshita, M. *Solid State Commun.* **1986**, *57*, 453. (b) Awaga, K.; Sugano, T.; Kinoshita, M. *J. Chem. Phys.* **1986**, *85* (4), 2211−2218.

(3) Jamali, J. B.; Achiwa, N.; Mukai, K.; Suzuki, K.; Asano, T.; Ajiro, Y.; Matsuda, K.; Iwamura, H.; Kuwajima, S.; Soeijima, Y. *Mol. Cryst. Liq. Cryst.* **1999**, *334*, 121−130.
(4) Mukai, K.; Suzuki, K.; Ohara, K.; Jamali, J. B.; Achiwa, N. *J. Phys. Soc. Jpn.* **1999**, *68*, 3078−3085.
(5) (a) Mukai, K. *Chem. Phys. Lett.* **1999**, *311*, 446−452. (b) Mukai, K.; Yanagimoto, M.; Shimobe, Y.; Kindo, K.; Hamamoto, T. *J. Phys. Chem. B* **2002**, *106*, 3687−3695. (c) Mukai, K.; Yanagimoto, M.; Narimatsu, S.; Maruyama, H.; Narumi, Y.; Kindo, K. *J. Phys. Soc. Jpn.* **2002**, *71*, 2539−2545. (d) Mukai, K.; Yanagimoto, M.; Tanaka, S.; Mito, M.; Kawae, T.; Takeda, K. *Polyhedron* **2003**, *22*, 2091−2098. (e) Mukai, K.; Yanagimoyo, M.; Tanaka, S.; Mito, M. *J. Phys. Soc. Jpn.* **2003**, *72*, 2312−2316. (f) Mito, M.; Tanaka, S.; Kawae, T.; Takeda, K.; Yanagimoto, M.; Mukai, K. *Phys. B* **2003**, *329*, 1150−1151.
(6) Murata, H.; Mague, J. T.; Aboaku, S.; Yoshioka, N.; Lahti, P. M. *Chem. Mater.* **2007**, *19*, 4111−4113.
(7) (a) Murata, H.; Delen, Z.; Lahti, P. M. *Chem. Mater.* **2006**, *18*, 2625−2627. (b) Murata, H.; Miyazaki, Y.; Inaba, A.; Paduan-Filho, A.; Bindilatti, V.; Oliveira, N. F. Jr.; Delen, Z.; Lahti, P. M. *J. Am. Chem. Soc.* **2008**, *130*, 186−194.
(8) (a) Yoshioka, N.; Irisawa, M.; Mochizuki, Y.; Kato, T.; Inoue, H.; Ohba, S. *Chem. Lett.* **1997**, 251−252. (b) Yoshioka, N.; Irisawa, M.; Mochizuki, Y.; Aoki, T.; Inoue, H. *Mol. Cryst. Liq. Cryst.* **1997**, *306*, 403−408. (c) Yamaguchi, K.; Kawakami, T.; Oda, A.; Yoshioka, Y. In *Magnetic Properties of Organic Materials*; Lahti, P. M., Ed.; Marcel Dekker: New York, 1999.
(9) (a) Sugano, T.; Blundell, S. J.; Hayes, W.; Day, P. *Polyhedron* **2003**, *22*, 2343. (b) Sugano, T.; Blundell, S. J.; Hayes, W.; Day, P. *J. Phys. IV* **2004**, *114*, 651. (c) Sharmin, S.; Blundell, S. J.; Sugano, T.; Ardavan, A. *Polyhedron* **2005**, *24*, 2360.
(10) *SAINT+*, Version 7.03; Bruker-AXS: Madison, WI, 2004.
(11) Sheldrick, G. M. *SADABS*, Version 2.05; University of Göttingen: Göttingen, Germany, 2002.
(12) Sheldrick, G. M. *Acta Crystallogr.* **2008**, *A64*, 112−122 ; SHELXTL, Version 6.10; Bruker-AXS: Madison, WI, 2000.
(13) Oliveira, N. F. Jr.; Paduan-Filho, A.; Salinas, S. R.; Becerra, C. C. *Phys. Rev. B* **1978**, *18*, 6165−6177.
(14) (a) Swank, D. D.; Landee, C. P.; Willet, R. D. *Phys. Rev. B* **1979**, *20*, 2154−2162. (b) Baker, G. A. Jr.; Rushbrooke, G. S.; Gilbert, H. E. *Phys. Rev.* **1964**, *135*, A1272−1277.
(15) Sugano, T.; Blundell, S. J.; Lancaster, T.; Pratt, F. L.; Mori, H. *Phys. Rev. B* **2010**, *82*, 180401(R).
(16) Frisch, M. J.; et al. *Gaussian 09*, Revision B.01; Gaussian, Inc: Wallingford, CT, 2010.
(17) Taylor, P. S.; Lahti, P. M. *Cambridge Structure Databank Code REVPAK* **2006**.
(18) (a) Stibrany, R. T.; Potenza, J. A.; Schugar, H. J. *Cambridge Structure Databank Code BZDMAZ02* **2001**. (b) Escande, A.; Galigne, J. L. *Acta Crystallogr. B* **1974**, *30*, 1647−1648. (c) Dik-Edixhoven, C. J.; Schenk, H.; van der Meer, H. *Cryst. Struct. Commun.* **1973**, *2*, 23−24.
(19) (a) Collings, J. C.; Smith, P. S.; Yufit, D. S.; Batsanov, A. S.; Howard, J. A. K.; Marder, T. B. *CrystEngComm* **2004**, *6*, 25−28. (b) Dunitz, J. D.; Gavezzotti, A.; Schweizer, W. B. *Helv. Chim. Acta* **2003**, *86*, 4073−4092. (c) Collings, J. C.; Roscoe, K. P.; Robins, E. G.; Batsanov, A. S.; Stimson, L. M.; Howard, J. A. K.; Clark, S. J.; Marder, T. B. *New J. Chem.* **2002**, *26*, 1740−1746. (d) Collings, J. C.; Roscoe, K. P.; Thomas, R. Ll.; Batsanov, A. S.; Stimson, L. M.; Howard, J. A. K.; Marder, T. B. *New J. Chem.* **2001**, *25*, 1410−1417. (e) Williams, J. H.; Cockcroft, J. K.; Fitch, A. N. *Angew. Chem., Int. Ed. Engl.* **1992**, *31*, 1655−1657. (f) Patrick, C. R.; Prosser, G. S. *Nature* **1960**, *187*, 1021.
(20) Allen, C.; Haynes, D. A.; Pask, C. M.; Rawson, R. M. *CrystEngComm* **2009**, *11*, 2048−2050.
(21) Some recent organic magnetic systems have not only a strong FM chain interaction, but also significant interchain interactions: (a) Zakrassov, A.; Shteiman, V.; Sheynin, Y.; Tumanskii, B.; Botoshansky, M.; Kapon, M.; Keren, A.; Kaftory, M.; Vosc, T. E.; Miller, J. S. *J. Mater. Chem.* **2004**, *14*, 1827−1837. (b) Yu, X.; Mailman, A.; Dube, P. A.; Abdeljalil Assoud, A.; Oakley, R. T. *Chem. Commun.* **2011**, *47*, 4655−4657.
(22) Seber, G.; Halder, G. J.; Schlueter, J. A.; Lahti, P. M. *Cryst. Growth Des.* **2011**, *11*, 4261−4266.
(23) Macrae, C. F.; Bruno, I. J.; Chisholm, J. A.; Edgington, P. R.; McCabe, P.; Pidcock, E.; Rodriguez-Monge, L.; Taylor, R.; van de Streek, J.; Wood, P. A. *J. Appl. Crystallogr.* **2008**, *41*, 466−470 ; Program Mercury is available from the Cambridge Crystallographic Data Centre..